

1
2
3
4 **1 Chemical Oxidation of Ibuprofen in the presence of iron species at near**
5
6
7 **2 neutral pH**
8
9

10 3
11
12 4
13
14 5
15
16
17 6 N. Sabri¹, K. Hanna², V. Yargeau^{1*}
18
19 7
20
21 8
22

23
24 ¹Department of Chemical Engineering, McGill University, 3610 University Street,
25
26 Montreal, Quebec H3A2B2, Canada.
27
28

29 9
30
31 ²Ecole Nationale Supérieure de Chimie de Rennes, UMR CNRS 6226 "Sciences
32
33 Chimiques de Rennes" Chimie et Ingénierie des Procédés, Avenue du Général Leclerc,
34
35 35708 Rennes, France.
36
37
38
39
40

41 13
42
43 14
44
45
46 15
47
48 **16 Corresponding author:** Prof. Viviane Yargeau, Department of Chemical Engineering,
49
50 McGill University, 3610 University Street, Montreal, Canada.
51

52
53 18 Email: viviane.yargeau@mcgill.ca; Tel: 514-398-2273; Fax: 514-398-6678.
54
55
56 19
57
58
59
60
61
62
63
64
65

1
2
3
4
5
6
7
8
9
10
11
12
13
14
15
16
17
18
19
20
21
22
23
24
25
26
27
28
29
30
31
32
33
34
35
36
37
38
39
40
41
42
43
44
45
46
47
48
49
50
51
52
53
54
55
56
57
58
59
60
61
62
63
64
65

20 **Abstract**

21
22 The objective of this work was to evaluate the removal of ibuprofen (IBP) using the
23 oxidants hydrogen peroxide (H₂O₂) and sodium persulfate (Na₂S₂O₈). The ability of
24 magnetite (Fe₃O₄) to activate persulfate (PS) and H₂O₂ for the oxidation of IBP at near
25 neutral pH was evaluated as well. The use of soluble Fe²⁺ to activate H₂O₂ and Na₂S₂O₈
26 was also investigated. H₂O₂ and Na₂S₂O₈ were inactive during the sixty-minute
27 experiments when used alone. However, activation using Fe²⁺ increased the removal to
28 95% in the presence of H₂O₂ (Fenton reaction) and 63% in the presence of Na₂S₂O₈ at pH
29 6.6. Chemical oxygen demand (COD) removal was also greater for Fenton oxidation
30 (65%) than for iron-activated PS oxidation (25%). Activation of H₂O₂ and PS by Fe₃O₄
31 was only observed at a high oxidant concentration and over 48 hrs of reaction time. A
32 second order rate kinetic constant was determined for H₂O₂ (3.0*10⁻³ M⁻¹ s⁻¹) and
33 Na₂S₂O₈ (1.59*10⁻³ M⁻¹ s⁻¹) in the presence of Fe₃O₄. Finally, several of the degradation
34 products formed during oxidation of IBP in the presence of H₂O₂ and Na₂S₂O₈ (activated
35 by Fe²⁺) were identified. These include oxalic acid, pyruvic acid, formic acid, acetic acid,
36 4-acetylbenzoic acid, 4-isobutylacetophenone (4-IBAP) and oxo-ibuprofen.

37
38
39 **Keywords:** Ibuprofen; oxidation; persulfate; Fenton; magnetite.

1
2
3
4 **40 1. Introduction**
5
6 41

7
8 42 Ibuprofen (2-(4-Isobutylphenyl) propanoic acid) is a non steroidal anti inflammatory,
9
10 43 antipyretic and analgesic drug. It is widely used for the treatment of inflammatory
11
12 44 disorders such as rheumatoid arthritis and for pain relief. In 1984 it was approved as an
13
14 45 over the counter drug and since then, non-prescription sales have tripled in North
15
16 46 America (Caviglioli et al., 2002). IBP is degraded in the human body into its principal
17
18 47 metabolites hydroxy-IBP, carboxy-IBP and to carboxy-hydratropic acid (Buser et al.,
19
20 48 1999; Fent et al., 2006), which have been found together with IBP in raw sewage
21
22 49 (Heberer, 2002) . In Canada, IBP and one of its metabolites have been detected in the
23
24 50 effluent of a primary wastewater treatment plant at concentrations greater than 500 ng L⁻¹
25
26 51 (Gagnon and Lajeunesse, 2008) while in Europe and the US, concentrations of up to 10
27
28 52 µg L⁻¹ were detected (Méndez-Arriaga et al., 2010; Pomati et al., 2004; Zorita et al.,
29
30 53 2009). There is currently no quantified limit to the discharge of IBP in wastewater from
31
32 54 manufacturing plants in Canada. However, considering that some physiological changes
33
34 55 such as growth inhibition of a Macrophyte species (Lemna Minor) and stimulated
35
36 56 production of the stress hormone abscisic acid in Lemna Minor(Pomati et al., 2004) have
37
38 57 been linked to IBP, more stringent regulations are expected in the near future. Simple,
39
40 58 efficient and cost-effective treatment options for the wash-water of vessels used in the
41
42 59 production process of IBP-containing pills will thus become essential to the
43
44 60 pharmaceutical industry. Various oxidation processes have been investigated for the
45
46 61 removal of IBP in water but their efficiencies of removal have varied from no removal to
47
48 62 complete removal (Caviglioli et al., 2002; Huber et al., 2003; Huber et al., 2005; Lee and
49
50 63 von Gunten, 2009; Madhavan et al., 2010; Méndez-Arriaga et al., 2010; Méndez-Arriaga
51
52
53
54
55
56
57
58
59
60
61
62
63
64
65

1
2
3
4 64 et al., 2008; Skoumal et al., 2009). Furthermore, toxic transformation products were
5
6 65 formed in a few cases (Caviglioli et al., 2002; Madhavan et al., 2010; Méndez-Arriaga et
7
8
9 66 al., 2010). More work is thus still needed to identify the best treatment option(s) for IBP-
10
11 67 containing industrial wastewaters.
12
13
14 68

15
16 69 All past research pertaining to the removal of IBP by the Fenton process only considered
17
18 70 using soluble Fe^{2+} (traditional Fenton's reagent) and in most of these studies, low pH
19
20 71 conditions ($\text{pH} < 4$) were required to prevent the precipitation of iron (Méndez-Arriaga et
21
22 72 al., 2010; Skoumal et al., 2009). Unlike the classical Fenton process, the reaction of Fe-
23
24 73 bearing minerals with hydrogen peroxide (H_2O_2) can effectively improve the oxidation of
25
26 74 organic molecules at circumneutral pH. This has been demonstrated for other
27
28
29 75 contaminants such as 2,4,6-trinitrotoluene and phenol (Matta et al., 2007; Matta et al.,
30
31 76 2008a; Matta et al., 2008b) but has yet to be shown for IBP. The degradation of
32
33 77 pharmaceutical compounds by Fenton's reagent and a Fenton-like system has also been
34
35 78 reported at acidic conditions (Goi et al., 2008; Hofmann et al., 2007; Méndez-Arriaga et
36
37 79 al., 2010; Skoumal et al., 2009). However the removal of IBP at neutral pH, which is less
38
39 80 abrasive to the environment, would be more appealing for applications in the treatment of
40
41
42
43 81 wastewater or wash water that is produced in IBP processing plants.
44
45
46
47
48 82

49
50 83 Persulfate (PS) was also proven to be very useful for the elimination of contaminants
51
52 84 such as diphenylamine, trichloroethylene, benzene, toluene, ethyl benzene and xylene in
53
54 85 aqueous and soil slurries (Liang et al., 2004a; Liang et al., 2004b; Liang et al., 2008).
55
56
57 86 However, currently only one study investigated the use of PS or activated-PS for the
58
59
60
61
62
63
64
65

1
2
3
4
5
6
7
8
9
10
11
12
13
14
15
16
17
18
19
20
21
22
23
24
25
26
27
28
29
30
31
32
33
34
35
36
37
38
39
40
41
42
43
44
45
46
47
48
49
50
51
52
53
54
55
56
57
58
59
60
61
62
63
64
65

87 elimination of a different pharmaceutical product, sulfamonomethoxine (Yan et al.,
88 2010). Although the activation of PS by soluble iron to form a sulfate radical ($\text{SO}_4^{\bullet-}$) has
89 been previously reported, the initiation of PS decomposition by iron oxide minerals has
90 been scarcely investigated (Ahmad et al., 2010; Yan et al., 2010).

91

92 Minerals like ferrihydrite, goethite, manganese oxide and clay were used to activate the
93 oxidation reaction of organic compounds (Ahmad et al., 2010). Fe^{II} -bearing minerals like
94 magnetite (Fe_3O_4) were found to be the most effective catalyst as compared to the only
95 Fe^{III} oxides for heterogeneous catalytic oxidation of organic pollutants (Ahmad et al.,
96 2010; Matta et al., 2007; Matta et al., 2008b; Xue et al., 2009b; Xue et al., 2009c). In
97 addition, Fe_3O_4 exhibited excellent structural and catalytic stabilities. Fe_3O_4 can be
98 magnetically recovered and re-used for several oxidation cycles; it is abundant in
99 environmental settings and has a low solubility in aqueous solution (Schwertmann and
100 Cornell, 2000; Xue et al., 2009a; Xue et al., 2009c). To date, the use of Fe_3O_4 (the most
101 stable mixed valence oxide), to activate PS or H_2O_2 , has not been tested for IBP removal.

102

103 The objectives of this study were to (i) examine the oxidation of IBP by H_2O_2 and PS at
104 near neutral pH, (ii) test the ability of soluble Fe^{II} and Fe_3O_4 to activate H_2O_2 or PS, (iii)
105 determine the extent of mineralization and identify the degradation byproducts of IBP
106 oxidation.

107

108 **2. Materials and Methods**

109

1
2
3
4 **110 2.1. Chemicals**

5
6
7 111 Ibuprofen ($\geq 98\%$), magnetite powder (Fe_3O_4 , 98%), sodium persulfate ($\text{Na}_2\text{S}_2\text{O}_8$, 99%),
8
9 112 ammonium acetate ($\geq 99.9\%$) and iron chloride tetrahydrate ($\text{FeCl}_2 \cdot 4 \text{H}_2\text{O}$, $\geq 99\%$) were
10
11 113 purchased from Sigma-Aldrich. Hydrogen peroxide (H_2O_2 35% w/w) was purchased
12
13 114 from EMD Chemicals. HPLC grade methanol ($\geq 99.9\%$) and HPLC grade ammonium
14
15 115 acetate ($\geq 99.0\%$) were purchased from Fisher Scientific. Hydrochloric acid (HCl,
16
17 116 $\geq 99\%$), sodium chloride (NaCl, $\geq 99.5\%$), sodium hydroxide (NaOH, 0.1M), 4-
18
19 117 acetylbenzoic acid (98%), oxalic acid ($\geq 99\%$), 4-ethylbenzaldehyde (98%), formic acid
20
21 118 (98%), pyruvic acid (98%) and acetic acid (98%) were purchased from Sigma Aldrich.
22
23 119 Oxo-ibuprofen was purchased from Santa Cruz Biotechnology Inc., and 4-
24
25 120 isobutylacetophenone (4-IBAP, $> 96\%$) from TCI America. Nitrogen (N_2 , 99.99%) was
26
27 121 purchased from Megs.
28
29
30
31
32

33 122

34
35
36 **123 2.2. Characterization of iron (II, III) oxide**

37
38 124 The X-Ray Diffraction (XRD) data were collected with a D8 Bruker diffractometer
39
40 125 equipped with a monochromator and a position-sensitive detector to confirm the nature of
41
42 126 the oxide (Fe_3O_4) before and after the oxidative treatment. The X-ray source was a Co
43
44 127 anode ($\lambda = 0.17902 \text{ nm}$). The diffractogram was recorded in the $3\text{-}64^\circ 2\theta$ range, with a
45
46 128 0.0359° step size and a collecting of 3s per point. The particle size distribution of Fe_3O_4
47
48 129 was measured using a Mastersizer 2000 from Malvern Instruments. The Tristar 3000
49
50 130 from Quantachrome Instruments was used to determine the specific surface area of Fe_3O_4
51
52 131 by Nitrogen Brunauer-Emmett-Teller (N_2 -BET) analysis. The point of zero charge (pzc)
53
54 132 of Fe_3O_4 was determined through potentiometric titrations (Xue et al., 2009a).
55
56
57
58
59
60
61
62
63
64
65

1
2
3
4 133

5
6 134 Scanning Electron Microscopy (SEM) analysis was used to determine the morphology of
7
8
9 135 the purchased Fe_3O_4 . The SEM images were collected with a HITACHI FEG 54800
10
11 136 apparatus operated with a beam current of 3 pA and an accelerating voltage of 20 kV
12
13
14 137 (analyzed microvolume of $\sim 6 \mu\text{m}^3$). The solid powder was glued on an adhesive surface
15
16 138 and metalized with a thin layer of gold.
17
18

19 139

20
21 140 Transmission Electron Microscopy (TEM) analysis was also performed to obtain
22
23 141 information regarding the morphology, the size, shape and arrangement of the particles.
24
25 142 TEM observations were carried out with a Philips CM20 TEM (200 kV) coupled with an
26
27 143 EDAX energy dispersive X-ray spectrometer (EDXS). The solid powder was re-
28
29 144 suspended in 2 mL ethanol under ultrasonication and a drop of suspension was
30
31 145 evaporated on a carbon-coated copper grid which was placed on filter paper for analysis.
32
33

34 146

35 36 37 38 147 **2.3. Edge sorption and sorption isotherms**

39
40 148 Edge sorption experiments were conducted to determine the effect of pH on IBP sorption
41
42 149 onto Fe_3O_4 . A solution with final concentrations of 0.1 mM IBP and 1 g L^{-1} of Fe_3O_4 ([Fe
43
44 150 total] = 13 mM) was prepared in 10 mM NaCl (NaCl was used as the supporting
45
46 151 electrolyte). The pH was then adjusted using either HCl or NaOH. For each pH value, 3
47
48 152 ml samples were extracted and filtered through $0.22 \mu\text{m}$ polyvinylidene fluoride (PVDF)
49
50 153 syringe filters (Millipore) that were previously shown not to sorb IBP. A UV-visible
51
52 154 spectrophotometer (Agilent 8543 spectrophotometer) was used to determine the IBP
53
54
55
56
57
58
59
60
61
62
63
64
65

1
2
3
4 155 concentration in solution at 273 nm and the adsorbed amount was calculated by the
5
6 156 depletion method (Matta et al., 2007).
7
8

9 157

10
11 158 Sorption isotherms were determined at 20°C. Variable initial IBP concentrations (0-0.5
12
13 159 mM) were prepared with Fe₃O₄ (final concentration of 1 g L⁻¹) at pH 6.6 ± 0.2. As before,
14
15 160 the IBP solutions were prepared in 10mM NaCl. Before analysis, the suspensions were
16
17 161 centrifuged, filtered and analyzed by UV-visible spectroscopy as previously described.
18
19
20

21 162

22 23 163 **2.4. Oxidation Experiments**

24
25 164 H₂O₂ and Na₂S₂O₈ were used to degrade a 0.1 mM solution of IBP (concentration in
26
27 165 reverse osmosis water, representative of levels observed in industrial wastewater) in the
28
29 166 presence and absence of both Fe²⁺ and Fe₃O₄. Experiments for optimization of oxidant
30
31 167 concentration (H₂O₂ and Na₂S₂O₈) were first conducted by varying the oxidant
32
33 168 concentration between 1 mM and 10 mM in the presence and absence of 1 mM of Fe²⁺.
34
35 169 Replicates were then carried out under the optimal oxidant concentration (in absence or
36
37 170 presence of the iron species) in a 250 ml beaker sealed with parafilm and covered with
38
39 171 aluminum foil to prevent any photo-transformation. The experiments were conducted at
40
41 172 pH of 6.6 ± 0.2. 3 ml samples were withdrawn at selected time intervals for 60 minutes
42
43 173 and filtered using 0.22 µm syringe filters and analyzed.
44
45
46
47
48
49

50 174

51
52
53 175 For the oxidation experiments using Fe₃O₄, Fe₃O₄ was added at a concentration of 1 g L⁻¹
54
55 176 ([Fe total] = 13 mM) before the experiments were initiated. When Fe²⁺ was used, iron
56
57 177 chloride tetrahydrate FeCl₂*4 H₂O was added to the IBP solution to obtain a
58
59
60
61
62
63
64
65

1
2
3
4 178 concentration of 1 mM of Fe^{2+} . N_2 was bubbled in the solution to prevent the oxidation of
5
6 179 Fe^{2+} to Fe^{3+} prior to commencing the experiment and throughout.
7
8

9 180

10
11 181 In order to determine the role of Fe_3O_4 in the kinetic investigation of IBP removal,
12
13 182 oxidation experiments were also carried out using higher oxidant concentrations (10 mM)
14
15 183 over a longer time frame (48 hrs).
16
17
18

19 184

20 21 185 **2.5. Analytical Methods**

22
23 186 Residual IBP concentration were monitored using High Performance Liquid
24
25 187 Chromatography (HPLC) (Agilent Technologies 1200 series) equipped with an Eclipse
26
27 188 XDB C-18 (5 μm , 4.6 mm X 250 mm) column (Agilent Technologies) using a diode
28
29 189 array detector at a wavelength of 220 nm and 254 nm. Mobile phases consisted of
30
31 190 methanol and ammonium acetate (20 mM adjusted to pH 3.0 using formic acid). The
32
33 191 flow rate was 0.7 ml/min. The gradient used was the following; 0 min = 60% B, 3% A, 2
34
35 192 min = 67% B, 3% A, 4 min = 74% B, 3% A, 6 min = 81% B, 3% A, 8 min = 88% B, 3%
36
37 193 A, 10 min = 95% B, 3% A, 12 min = 97% B, 3% A, 25 min = 97% B, 3% A. Where A
38
39 194 is ammonium acetate, B is methanol and the remainder is reverse osmosis water.
40
41
42
43
44
45

46 195

47
48 196 The limit of detection of IBP of this method was 0.1 mg L^{-1} ($0.5 \mu\text{M}$). The products
49
50 197 identification was carried out by comparison with standards analyzed using a mass
51
52 198 spectrometer (MDS/Sciex QTrap mass spectrometer) equipped with a TurboIon Spray
53
54 199 ionization source operated in positive and negative ion mode.
55
56

57
58 200
59
60
61
62
63
64
65

1
2
3
4 201 The extent of mineralization was estimated using Chemical Oxygen Demand (COD)
5
6 202 measured using a HACH Digital Reactor Block (DRB 200), a HACH spectrophotometer
7
8
9 203 (DR/2500) and low range digestion vials (0-150 mg L⁻¹). Ferrozine method was used to
10
11 204 quantify the amount of Fe²⁺ (Kostka and N., 1998; Lovley and P., 1986). Total Fe was
12
13
14 205 determined using Inductively Coupled Plasma Atomic Emission Spectroscopy (ICP-
15
16 206 AES) (Thermo Trace Scan equipped with a mini-crossflow nebulizer from SCP Science
17
18
19 207 and a baffled quartz cyclonic spray chamber).
20
21
22

23
24
25
26 208

27 209 **3. Results and Discussion**

28
29
30
31 210

32 211 **3.1. Characterization of Fe₃O₄**

33 212 The XRD diffractogram of Fe₃O₄ is shown in Figure 1a. Five diffraction peaks at 2θ =
34 213 21.2°, 35°, 41.2°, 50.4° and 62.8° could be assigned to Fe₃O₄, (Schwertmann and Cornell,
35 214 2000). The d-space values of these main peaks were 2.53, 2.96, 2.09, 4.85 and 1.71 Å,
36 215 which may respectively correspond to the more intense lines of Fe₃O₄; 311, 220, 400, 111
37
38 216 and 422. Fe₃O₄ is the only pure oxide of mixed valence and is usually represented by the
39 217 formula (Fe³⁺)_{tet}[Fe³⁺Fe²⁺]_{oct}O₄ (Xue et al., 2009a). It has a cubic spinel structure with
40
41 218 iron in both tetrahedral and octahedral sites. The XRD diffractogram recorded at the end
42
43 219 of oxidation reaction was found to be similar to that recorded before reaction, indicating
44
45 220 good stability of Fe₃O₄ during the oxidation process. The surface area determined by
46
47
48 221 BET method was 8.0 m² g⁻¹. The pzc value estimated from potentiometric titration was
49
50
51 222 around 9.
52
53
54
55
56
57
58 223

59
60
61
62
63
64
65

1
2
3
4 224 SEM image shows that the Fe_3O_4 particles are highly aggregated and exhibit irregular
5
6 225 shapes (Figure 1b). The size of the particles is non-uniform and ranges between ~ 100
7
8
9 226 and ~ 400 nm. If we consider that the particles are spherical, the radius of these particles
10
11 227 ($\rho = 5.15 \times 10^6 \text{ g m}^{-3}$) can be related to the surface area as $A = 6/(\rho d) = 8 \text{ m}^2 \text{ g}^{-1}$. Thus, the
12
13 228 average diameter calculated assuming a spherical shape is ~ 150 nm.
14
15
16
17 229

18
19 230 TEM image (Figure 1c) indicates that the Fe_3O_4 particles are more or less rhombohedral
20
21 231 in shape, with crystals varying between 100 and 300 nm in length. TEM combined with
22
23 232 EDXS yields an elemental analysis of the sample. Elemental ratios can be calculated by
24
25 233 EDXS and compared with known mineralogical compositions. EDX microanalyses of
26
27 234 samples before and after oxidation reactions showed the characteristic Fe/O ratio of
28
29 235 Fe_3O_4 .
30
31
32
33
34 236

36 237 **3.2. Sorption of IBP onto Fe_3O_4**

37
38 238 The effect of varying the initial solution pH value (3-9) on the adsorption of IBP is
39
40 239 illustrated in Figure 2a. Sorption of IBP onto the iron oxide decreases sharply at pH
41
42 240 values greater than 5. The observed sorption behavior can be attributed to a combination
43
44 241 of pH-dependent speciation of IBP ($\text{pK}_a = 4.54$) and surface charge characteristics of the
45
46 242 Fe_3O_4 ($\text{pzc}=9$). Based upon surface charging, adsorption is high at low pH values and
47
48 243 then decreases when pH increases. The charge repulsion is expected at high pH where the
49
50 244 sorbate and sorbent are both negatively charged. Such sorption behavior has also been
51
52 245 observed for some organic acid complexation on oxide surfaces (Evanko and Dzombak,
53
54 246 1999). In these studies, the adsorption envelope of monoprotic organic acids bound to
55
56
57
58
59
60
61
62
63
64
65

1
2
3
4 247 iron oxide by surface complexation typically showed maximum adsorption at a pH near
5
6 248 their corresponding pK_a .

7
8
9 249

10
11 250 Sorption isotherms were obtained to evaluate the effect of IBP concentration on sorption
12
13
14 251 to Fe_3O_4 (Figure 2b). The experimental isotherm data were fitted to the equations of
15
16 252 Langmuir and Freundlich by applying linear regression analysis. One way to assess the
17
18
19 253 goodness of fit of experimental isotherm data to these equations is to check the regression
20
21 254 coefficients obtained during the regression analysis. On the basis of regression
22
23
24 255 coefficient, the curves were shown a best fit with Freundlich isotherm at a low range of
25
26 256 solute concentration (0-50 $\mu\text{mol/L}$). The Freundlich equation has been used in the
27
28
29 257 following form:

30
31 258

32
33 259
$$Q = K_F C_e^{1/n} \quad (1)$$

34
35
36 260 Where Q ($\mu\text{mol/m}^2$) is the sorbed concentration, C_e ($\mu\text{mol/L}$) is the equilibrium
37
38 261 concentration at the end of the experiment and K_F and $1/n$ are Freundlich constants. A
39
40
41 262 plot ($R^2 = 0.98$) of $\log Q$ versus $\log C_e$ enabled the determination of the Freundlich
42
43 263 constants: $K_F = 0.0082$ and $1/n = 0.84$.

44
45
46 264

47
48 265 **3.3. Oxidation of IBP**

49
50
51 266 The first objective of the oxidation experiments was to optimize the concentration of
52
53 267 H_2O_2 and $Na_2S_2O_8$ in presence of 1 mM of Fe^{2+} . Fe^{2+} concentration was chosen within
54
55 268 the range reported in literature for Fenton and PS oxidation ($[Fe^{2+}] = 0.5\text{mM} - 5\text{mM}$)
56
57
58 269 (Liang et al., 2004a; Méndez-Arriaga et al., 2010). The optimization of H_2O_2

1
2
3
4 270 concentration in the 1 to 10 mM range at $\text{pH } 6.6 \pm 0.2$ is illustrated in Figure 3a. In the
5
6 271 absence of iron species, an additional 15 % removal was observed when the
7
8 272 concentration of H_2O_2 was increased by 10 fold (from 1 mM to 10 mM). However, in the
9
10 273 presence of Fe^{2+} , increasing H_2O_2 concentration had no effect on the removal of IBP.
11
12
13
14 274 Therefore, the value of 1 mM was chosen for the rest of the experiments.
15

16 275
17
18 276 Optimization experiments for PS oxidation were conducted by varying $\text{Na}_2\text{S}_2\text{O}_8$
19
20 277 concentrations (0.5 mM-2.57 mM) alone and in the presence of a fixed Fe^{2+} concentration
21
22 278 (Figure 3b). Fe^{2+} was set at 1 mM in accordance with literature and more importantly, in
23
24 279 order to allow comparison to the Fenton experiments. As illustrated in Figure 3b, at pH
25
26 280 6.6 ± 0.2 no difference in removal was observed between 1 mM and 2.57 mM of PS. Fe^{2+}
27
28
29 281 content was measured at the end of the experiment using the Ferrozine method. None was
30
31 282 detected after 60 minutes of treatment, indicating that all Fe^{2+} had been completely
32
33 283 reacted. Therefore, 1 mM of $\text{Na}_2\text{S}_2\text{O}_8$ or H_2O_2 was selected as optimal concentration for
34
35 284 all oxidation experiments.
36
37
38
39
40
41 285

42
43 286 As shown in Figure 4a, 1 mM of H_2O_2 used alone or in the presence of Fe_3O_4 led to
44
45 287 minimal removal (<1%) over 60 min of reaction time. The oxidation ability of H_2O_2 was
46
47 288 strongly enhanced by adding a small quantity of readily available Fe^{2+} which produces
48
49
50 289 Fe^{3+} , hydroxyl radicals (OH^\bullet) and hydroxide anions (OH^-) as demonstrated in previous
51
52
53 290 studies (Méndez-Arriaga et al., 2010; Poyatos et al., 2009; Weiss, 1952). A removal of
54
55 291 95% was obtained after a reaction time of 60 minutes under these conditions.
56
57
58

59 292
60
61
62
63
64
65

1
2
3
4 293 Mendez-Arriaga et al. (2010) reported that IBP ($C_o = 0.87\text{mM}$) subjected to varying
5
6 294 concentrations of H_2O_2 ($8.7 \times 10^{-4} \text{ mM} - 8.7 \text{ mM}$) at a pH and temperature similar to the
7
8
9 295 research presented here resulted in no removal after 2 hours of treatment time. However,
10
11 296 they showed that increasing Fe^{2+} concentrations ($0.15\text{-}1.2 \text{ mM}$) led to higher IBP
12
13 297 degradation with an initial H_2O_2 concentration fixed at 0.32 mM . The maximum removal
14
15 298 achieved was 60% under the following conditions: $\text{IBP} = 0.87 \text{ mM}$, $\text{Fe}^{2+} = 1.2 \text{ mM}$ and
16
17 299 $\text{H}_2\text{O}_2 = 0.32 \text{ mM}$. This is significantly less than the 95% removal observed in the work
18
19 300 presented herein. This could be attributed to two factors: 1) the lower ratio of H_2O_2 : Fe^{2+}
20
21 301 ($1:4$) which would lead to a reduced generation of OH^\bullet and 2) the higher initial
22
23
24
25 302 concentration of IBP (~ 9 times greater than the IBP concentration used in this work)
26
27
28 303 leading to reduced number of oxidizing species per mole of IBP.
29
30
31

32 304
33
34 305 During PS oxidation, negligible removal was observed in the absence of iron species and
35
36 306 in the presence of Fe_3O_4 while a 63% removal was obtained in presence of Fe^{2+} after 60
37
38 307 min (Figure 4b). The highly significant impact of adding Fe^{2+} can be explained as
39
40 308 follows. The PS anion ($\text{S}_2\text{O}_8^{2-}$) has a high redox potential ($E^\circ = 2.01 \text{ V}$) and is chemically
41
42 309 activated by Fe^{2+} to form the sulfate radical ($\text{SO}_4^{\bullet-}$), which is an even stronger oxidant (E°
43
44 310 $= 2.4$) (Liang et al., 2004a). $\text{SO}_4^{\bullet-}$ can also react with water or OH^- to generate OH^\bullet
45
46
47
48 311 (Peyton, 1993). Furthermore, OH^\bullet can initiate a series of propagation reactions that
49
50
51 312 generate perhydroxyl radicals, superoxide radical anions and hydroperoxide anions
52
53
54
55 313 (Monahan et al., 2005). However, Fe_3O_4 cannot activate PS to form $\text{SO}_4^{\bullet-}$ under our
56
57
58
59
60
61
62
63
64
65

1
2
3
4 314 experimental conditions (Figure 4b). Yan et al. (2010) reported that Fe_3O_4 used at a high
5
6 315 concentration hindered the PS oxidation of sulfamonomethoxine. In the present work, the
7
8
9 316 high concentration of Fe_3O_4 may have scavenged the $\text{SO}_4^{\bullet-}$, leading to the transformation
10
11
12
13 317 of the radical into the sulfate anion (SO_4^{2-}). This scavenging effect was also observed in
14
15
16 318 previous studies for the heterogeneous Fenton reaction at a high loading of Fe_3O_4 (Xue et
17
18 319 al., 2009a; Xue et al., 2009b).

20
21 320
22
23 321 An important observation made during these experiments was that Fe^{2+} quickly oxidized
24
25 322 for an almost instantaneous oxidation of IBP; then, the reaction was stalled. This behavior
26
27 323 was also observed in the studies of Liang et al. (2004a & 2008) for the PS oxidation of
28
29 324 trichloroethylene (TCE) and benzene-toluene-ethylbenzene-xylene (BTEX) compounds.

30
31
32
33 325 It was hypothesized that this behavior was due to either the destruction of $\text{SO}_4^{\bullet-}$ in the
34
35 326 presence of excess Fe^{2+} or the rapid conversion of Fe^{2+} to Fe^{3+} (Liang et al., 2004a; Liang
36
37 327 et al., 2008). The instantaneous change in color observed when PS was added and the
38
39 328 formation of an iron hydroxide precipitate ($\text{Fe}(\text{OH})_3$) within the first 3 minutes strongly
40
41 329 suggests that the oxidation of Fe^{2+} was very rapid. In addition, combination of $\text{SO}_4^{\bullet-}$ may
42
43
44
45
46
47 330 occur due to an excess of radicals being formed.

48
49 331
50
51
52 332 Note that kinetic rate constants cannot be determined for the above mentioned oxidation
53
54 333 experiments because the removal of IBP in the absence of iron species or presence of
55
56 334 Fe_3O_4 was insignificant over the studied reaction time. Furthermore, kinetic investigation
57
58
59
60
61
62
63
64
65

1
2
3
4 335 was also not considered in the presence of Fe^{2+} due to the rapidity of the reaction, making
5
6 336 it impossible to sample over the short reaction time. The following section discusses the
7
8
9 337 kinetic removal of IBP under an extended time frame (48 hrs) and using a higher initial
10
11 338 oxidant concentration in the presence of Fe_3O_4 .

12
13
14 339

15 16 340 **3.4. Kinetic of IBP removal using Fe_3O_4**

17
18
19 341 In order to determine the role of Fe_3O_4 on the kinetics of IBP removal, oxidation
20
21 342 experiments were carried out using a higher oxidant concentration (10 mM) over a longer
22
23 343 time frame (48 hrs) as proposed in a previous work (Xue et al., 2009a). As illustrated in
24
25 344 Figure 5, the removal of IBP by H_2O_2 alone is minimal (~20 %) which is in agreement
26
27 345 with previous studies (Méndez-Arriaga et al., 2010; Skoumal et al., 2009). Conversely,
28
29 346 H_2O_2 oxidation is significantly enhanced by the presence of Fe_3O_4 (~60%). This behavior
30
31 347 was also observed for IBP removal by PS, where the removal was increased from 58% to
32
33 348 73%. The increase in removal for both oxidants is due to the adsorption of IBP onto
34
35 349 Fe_3O_4 and to the increased formation of either $\text{SO}_4^{\bullet-}$ or OH^{\bullet} . This is a result of using
36
37 350 larger initial oxidant concentrations which target the IBP molecule due to the radicals
38
39 351 non-selective behavior.

40
41
42 352

43
44
45 353 To determine rate constants for Fe_3O_4 -activated H_2O_2 and $\text{Na}_2\text{S}_2\text{O}_8$, the raw data was fit
46
47 354 to a second order reaction;

48
49
50 355
$$k * t = \frac{1}{C_a} - \frac{1}{C_{ao}} \quad (2)$$

1
2
3
4 356 Where k is the rate order constant ($M^{-1} s^{-1}$), t is the time (s), C_{a0} is the initial concentration
5
6 357 of IBP and C_a (mM) is the remaining concentration of IBP (mM).
7
8

9 358

10
11 359 The rate constants for the removal of IBP by the oxidizing species formed were
12
13 360 determined to be: $1.59 \cdot 10^{-3} M^{-1} s^{-1}$ for PS and $3.0 \cdot 10^{-3} M^{-1} s^{-1}$ for H_2O_2 in the presence of
14
15
16 361 Fe_3O_4 . When comparing these results to those obtained by Huber et al. (2003) and Lee et
17
18
19 362 al. (2009), the second order rate constant for the reaction of OH^\bullet with IBP ($7.4 \times 10^9 M^{-1} s^{-1}$
20
21
22 363 ¹) is approximately 12 orders of magnitude greater than to $Na_2S_2O_8$ and H_2O_2 in presence
23
24
25 364 of Fe_3O_4 . No study has presented the reaction rate constant for IBP removal by $SO_4^{\bullet-}$. In
26
27
28 365 the case of PS and Fenton oxidation, we have seen that Fe_3O_4 can indeed promote the
29
30
31 366 formation of $SO_4^{\bullet-}$ and OH^\bullet , however this is hindered if the catalyst loading is too large
32
33
34
35 367 as these conditions lead to a scavenging effect. Additionally, H_2O_2 and PS are selective
36
37 368 oxidants. Lee et al. (2009) demonstrated that selective oxidants only react with some
38
39 369 electron-rich organic moieties, (such as phenols, anilines, olefins, and deprotonated-
40
41
42 370 amine) which are not present in IBP. Therefore the low reaction rate constants can be
43
44
45 371 justified by the scavenging effect of the radicals formed and the non-selective behavior of
46
47 372 the oxidants (Lee and von Gunten, 2009).
48

49 373

50 51 374 **3.5. COD abatement vs. time and identification of degradation products**

52
53
54 375 In order to determine the extent of mineralization, COD was determined in the absence of
55
56 376 iron species and in the presence of Fe^{2+} for both oxidants (H_2O_2 or $Na_2S_2O_8$). Figure 6
57
58
59 377 presents the average removal obtained with the error bars representing the minimum and
60
61
62
63
64
65

1
2
3
4 378 maximum values of the replicates. No COD removal was observed for H₂O₂ and PS
5
6 379 alone. The addition of Fe²⁺ enhanced the COD removal to 65% and 25% for H₂O₂ and
7
8
9 380 PS, respectively.

10
11 381

12
13
14 382 Different products were detected as new peaks on the HPLC chromatogram of the
15
16 383 samples collected during oxidation with Fe²⁺. Four of the most abundant degradation
17
18 384 products, detected at retention times of 4.6, 4.8, 8.8 and 10.1 minutes, were collected as
19
20
21 385 fractions. These fractions were analyzed by mass spectrometry (MS) by comparison with
22
23 386 standards of compounds reported in literature as potential degradation products of IBP.
24
25
26 387 Table 1 presents these products which were confirmed to be: 4-acetylbenzoic acid, oxalic
27
28 388 acid, oxo-ibuprofen and 4-isobutylacetophenone (4-IBAP). 4-IBAP has previously been
29
30
31 389 detected in the environment at the inlet and outlet of a tertiary sewage treatment plant in
32
33 390 Sweden (Zorita et al., 2009). Furthermore this product has proven to be quite toxic and
34
35
36 391 the subsequent effects of the compound on the central nervous system are well known
37
38 392 (Miranda et al., 1991). No information regarding the persistence or toxicity of 4-
39
40
41 393 acetylbenzoic acid and oxo-ibuprofen has been presented in literature.

42
43 394

44
45 395 Further MS analysis also confirmed the presence of formic acid, pyruvic acid and acetic
46
47
48 396 acid in the treated solution but the presence of 4-ethylbenzaldehyde, also proposed in
49
50
51 397 literature as a potential product, was not confirmed. However, 4-ethylbenzaldehyde is
52
53 398 known to have a sweet smell and during the oxidation experiments this type of odor was
54
55 399 frequently detected and may suggest that this volatile product was formed but did not
56
57
58 400 accumulate in the treated solution. One study determined the lethal dose (LD₅₀) on rats to

1
2
3
4 401 be 1970 mg kg⁻¹ of body weight (Adams et al., 2005). The value presented in literature is
5
6 402 not of concern because it is several orders of magnitude higher than what is produced
7
8
9 403 during oxidation. Acetic acid is thought to be formed from pyruvic acid degradation,
10
11 404 which has been determined to be a by-product of 4-IBAP. Oxalic acid is mainly formed
12
13
14 405 from the oxidative breakdown of the aryl moiety of aromatics and is largely formed from
15
16 406 oxidation of pyruvic and acetic acid. Furthermore, similarly to oxalic acid, formic acid is
17
18
19 407 an ultimate carboxylic acid since it is directly transformed into CO₂ (Adams et al., 2005;
20
21 408 Skoumal et al., 2009).

22
23 409
24
25
26 410 Due to the low concentration of the degradation products relative to the limit of detection
27
28 411 of the HPLC method used, it was not possible to investigate the persistence of the
29
30
31 412 degradation products formed. The peak area of only one degradation product, detected at
32
33 413 a retention time of 13.2 min, could be monitored with respect to time. As shown in Figure
34
35 414 7, this degradation product, which could not be identified by LC-MS, was continuously
36
37
38 415 removed over a period of 30 min even though IBP oxidation had terminated after 3 min
39
40
41 416 during Fe²⁺-activated PS oxidation. This suggests that there are still oxidizing species
42
43 417 present in solution, such as S₂O₈²⁻ which inevitably contributes to the removal of the
44
45 418 degradation products.

46
47 419
48
49
50 420 In the work of Cavliogli et al. (2002), it was noted that several degradation products of
51
52 421 IBP form during thermal and oxidative treatments (treatments include; KMnO₄, H₂O₂ and
53
54 422 K₂Cr₂O₇). Only three degradation products detected here were the same as those found in
55
56
57 423 Cavliogli et al. (2002), which were 4-acetylbenzoic acid, oxo-ibuprofen and 4-IBAP.
58
59
60
61
62
63
64
65

1
2
3
4 424 Mendez Arriaga et al. (2010) reported that hydroxylated byproducts were formed during
5
6 425 Fenton treatment and that decarboxylated and hydroxylated byproducts were formed
7
8
9 426 during photo-Fenton treatment (Méndez-Arriaga et al., 2010). Based on the products
10
11 427 identified in our study, especially formic acid, which can be formed from decarboxylation
12
13
14 428 of IBP, decarboxylation was thought to be the main mechanism of degradation.
15

16 429

19 430 **4. Conclusion**

21 431

23 432 The aim of this work was to test the ability of soluble Fe^{2+} and Fe_3O_4 to activate both
24
25 433 H_2O_2 and PS. H_2O_2 and $\text{Na}_2\text{S}_2\text{O}_8$ without activation had little effect on IBP removal.
26
27
28 434 When Fe^{2+} was introduced into the system, the removal was greatly enhanced. The
29
30
31 435 removal efficiency increased to 95% in the presence of H_2O_2 and to 63% in the presence
32
33 436 of $\text{Na}_2\text{S}_2\text{O}_8$ at pH 6.6. This behavior was also reflected in the COD results.
34

35
36 437 The $\text{Fe}_3\text{O}_4/\text{H}_2\text{O}_2$ system was also shown for the first time to effectively degrade IBP
37
38 438 through a heterogeneous Fenton reaction. The presence of Fe_3O_4 activated PS oxidation
39
40
41 439 of IBP through the possible formation of reactive species such as $\text{SO}_4^{\bullet-}$ and OH^{\bullet} . A
42
43
44 440 higher kinetic rate constant was found for the oxidation of IBP by H_2O_2 compared to PS
45
46
47 441 in the presence of magnetite. This is the first study to present the reaction rate constant
48
49
50 442 for IBP removal by the $\text{SO}_4^{\bullet-}$. Although the kinetics of Fenton-like and PS reactions are
51
52
53 443 slower than those of homogeneous oxidation reactions using Fe^{2+} , the use of Fe_3O_4 as an
54
55 444 iron source offers many advantages for engineering application purposes. First, Fe_3O_4 can
56
57
58 445 be used under a wide pH range, unlike homogeneous Fe^{2+} which has a risk of
59
60
61
62
63
64
65

1
2
3
4 446 precipitating out at high pH values. Secondly, due to its magnetic properties, Fe₃O₄
5
6 447 particles may be easily separated or recovered from aqueous solutions unlike Fe²⁺ which
7
8
9 448 can form iron sludges. In addition, Fe₃O₄ was shown to be re-usable for further oxidation
10
11 449 cycles without attrition and has a low loss of iron content. Furthermore, Fe₃O₄ has a good
12
13
14 450 structural stability during oxidation cycles at neutral pH (Xue et al., 2009a). Therefore it
15
16 451 can be hypothesized that re-use would be possible for IBP oxidation as well. The
17
18
19 452 relatively low cost, stability and reusability of Fe₃O₄ make it an environmentally friendly
20
21 453 catalyst to remediate an increasing number of environmental pollutants.
22

23
24 454

25 26 455 **Acknowledgements**

27
28 456

29
30
31 457 The authors would like to acknowledge the Natural Sciences and Engineering Research
32
33 458 Council of Canada (NSERC) and Eugenie Ulmer Lamothe Chemical Engineering Fund
34
35
36 459 (McGill University) for the financial support provided in this work. The authors would
37
38 460 also like to thank Hongxia Li at the Water Quality Centre at Trent
39
40
41 461 University for her help in identifying the degradation products.
42

43 462

44 45 463 **References**

46
47
48 464 Adams TB, Cohen SM, Doull J, Feron VJ, Goodman JI, Marnett LJ, et al. The FEMA
49 465 GRAS assessment of benzyl derivatives used as flavor ingredients. *Food and*
50 466 *Chemical Toxicology* 2005; 43: 1207-1240.
51 467 Ahmad M, Teel AL, Watts RJ. Persulfate activation by subsurface minerals. *Journal of*
52 468 *Contaminant Hydrology* 2010; 115: 34-45.
53 469 Buser H-R, Poiger T, MÄller MD. Occurrence and Environmental Behavior of the Chiral
54 470 Pharmaceutical Drug Ibuprofen in Surface Waters and in Wastewater.
55 471 *Environmental Science & Technology* 1999; 33: 2529-2535.
56
57
58
59
60
61
62
63
64
65

1
2
3
4
5
6
7
8
9
10
11
12
13
14
15
16
17
18
19
20
21
22
23
24
25
26
27
28
29
30
31
32
33
34
35
36
37
38
39
40
41
42
43
44
45
46
47
48
49
50
51
52
53
54
55
56
57
58
59
60
61
62
63
64
65

472 Caviglioli G, Valeria P, Brunella P, Sergio C, Attilia A, Gaetano B. Identification of
473 degradation products of Ibuprofen arising from oxidative and thermal treatments.
474 Journal of Pharmaceutical and Biomedical Analysis 2002; 30: 499-509.

475 Evanko CR, Dzombak DA. Surface Complexation Modeling of Organic Acid Sorption to
476 Goethite. Journal of Colloid and Interface Science 1999; 214: 189-206.

477 Fent K, Weston AA, Caminada D. Ecotoxicology of human pharmaceuticals. Aquatic
478 Toxicology 2006; 76: 122-159.

479 Gagnon C, Lajeunesse A. Persistence and fate of highly soluble pharmaceutical products
480 in various types of municipal waste water treatment plants. Waste Management
481 and the Environment IV 2008; 109: 799-807.

482 Goi A, Veressinina Y, Trapido M. Degradation of salicylic acid by Fenton and modified
483 Fenton treatment. Chemical Engineering Journal 2008; 143: 1-9.

484 Haber F, Weiss J. The Catalytic Decomposition of Hydrogen Peroxide by Iron Salts.
485 Proceedings of the Royal Society of London. Series A, Mathematical and Physical
486 Sciences 1934; 147: 332-351.

487 Heberer T. Occurrence, fate, and removal of pharmaceutical residues in the aquatic
488 environment: a review of recent research data. Toxicology Letters 2002; 131: 5-
489 17.

490 Hofmann J, Freier U, Wecks M, Hohmann S. Degradation of diclofenac in water by
491 heterogeneous catalytic oxidation with H₂O₂. Applied Catalysis B:
492 Environmental 2007; 70: 447-451.

493 Huber MM, Canonica S, Park G-Y, von Gunten U. Oxidation of Pharmaceuticals during
494 Ozonation and Advanced Oxidation Processes. Environmental Science &
495 Technology 2003; 37: 1016-1024.

496 Huber MM, Korhonen S, Ternes TA, von Gunten U. Oxidation of pharmaceuticals during
497 water treatment with chlorine dioxide. Water Research 2005; 39: 3607-3617.

498 Kostka JE, N. KH. Chapter 3: Isolation, cultivation, and characterization of iron- and
499 manganese-reducing bacteria. Oxford University Press, New York, 1998, pp. 468

500 Lee Y, von Gunten U. Oxidative transformation of micropollutants during municipal
501 wastewater treatment: Comparison of kinetic aspects of selective (chlorine,
502 chlorine dioxide, ferrate VI, and ozone) and non-selective oxidants (hydroxyl
503 radical). Water Research 2009; 44: 555-566.

504 Liang C, Bruell CJ, Marley MC, Sperry KL. Persulfate oxidation for in situ remediation
505 of TCE. I. Activated by ferrous ion with and without a persulfate-thiosulfate
506 redox couple. Chemosphere 2004a; 55: 1213-1223.

507 Liang C, Bruell CJ, Marley MC, Sperry KL. Persulfate oxidation for in situ remediation
508 of TCE. II. Activated by chelated ferrous ion. Chemosphere 2004b; 55: 1225-
509 1233.

510 Liang C, Huang C-F, Chen Y-J. Potential for activated persulfate degradation of BTEX
511 contamination. Water Research 2008; 42: 4091-4100.

512 Lovley DR, P. EJ. Organic Matter Mineralization with Reduction of Ferric Iron in
513 Anaerobic Sediments. Appl. Environ. Microbiol. 1986; 51: 6.

514 Matta R, Hanna K, Chiron S. Fenton-like oxidation of 2,4,6-trinitrotoluene using
515 different iron minerals. Science of The Total Environment 2007; 385: 242-251.

516 Matta R, Hanna K, Chiron S. Oxidation of phenol by green rust and hydrogen peroxide at
517 neutral pH. Separation and Purification Technology 2008a; 61: 442-446.

1
2
3
4
5
6
7
8
9
10
11
12
13
14
15
16
17
18
19
20
21
22
23
24
25
26
27
28
29
30
31
32
33
34
35
36
37
38
39
40
41
42
43
44
45
46
47
48
49
50
51
52
53
54
55
56
57
58
59
60
61
62
63
64
65

518 Matta R, Hanna K, Kone T, Chiron S. Oxidation of 2,4,6-trinitrotoluene in the presence
519 of different iron-bearing minerals at neutral pH. *Chemical Engineering Journal*
520 2008b; 144: 453-458.

521 Méndez-Arriaga F, Esplugas S, Giménez J. Degradation of the emerging contaminant
522 ibuprofen in water by photo-Fenton. *Water Research* 2010; 44: 589-595.

523 Méndez-Arriaga F, Torres-Palma RA, Pétrier C, Esplugas S, Gimenez J, Pulgarin C.
524 Ultrasonic treatment of water contaminated with ibuprofen. *Water Research* 2008;
525 42: 4243-4248.

526 Miranda MA, Morera I, Vargas F, Gómez-Lechón MJ, Castell JV. In vitro assessment of
527 the phototoxicity of anti-inflammatory 2-arylpropionic acids. *Toxicology in Vitro*
528 1991; 5: 451-455.

529 Monahan MJ, Teel AL, Watts RJ. Displacement of five metals sorbed on kaolinite during
530 treatment with modified Fenton's reagent. *Water Research* 2005; 39: 2955-2963.

531 Peyton GR. The free-radical chemistry of persulfate-based total organic carbon analyzers.
532 *Marine Chemistry* 1993; 41: 91-103.

533 Pomati F, Netting AG, Calamari D, Neilan BA. Effects of erythromycin, tetracycline and
534 ibuprofen on the growth of *Synechocystis* sp. and *Lemna minor*. *Aquatic*
535 *Toxicology* 2004; 67: 387-396.

536 Poyatos JM, Muñoz MM, Almecija MC, Torres JC, Hontoria E, Osorio F. Advanced
537 Oxidation Processes for Wastewater Treatment: State of the Art. *Water, Air, &*
538 *Soil Pollution* 2009.

539 Schwertmann U, Cornell RM. Magnetite. *Iron Oxides in the Laboratory: Preparation and*
540 *Characterization*. WILEY-VCH Verlag GmbH, Weinheim, 2000, pp. 135-140.

541 Skoumal M, Rodríguez RM, Cabot PL, Centellas F, Garrido JA, Arias C, et al. Electro-
542 Fenton, UVA photoelectro-Fenton and solar photoelectro-Fenton degradation of
543 the drug ibuprofen in acid aqueous medium using platinum and boron-doped
544 diamond anodes. *Electrochimica Acta* 2009; 54: 2077-2085.

545 Weiss J. The Free Radical Mechanism in the Reactions of Hydrogen peroxide. In: W.G.
546 Frankenburg VIK, Rideal EK, editors. *Advances in Catalysis*. Volume 4.
547 Academic Press, 1952, pp. 343-365.

548 Xue X, Hanna K, Abdelmoula M, Deng N. Adsorption and oxidation of PCP on the
549 surface of magnetite: Kinetic experiments and spectroscopic investigations.
550 *Applied Catalysis B: Environmental* 2009a; 89: 432-440.

551 Xue X, Hanna K, Deng N. Fenton-like oxidation of Rhodamine B in the presence of two
552 types of iron (II, III) oxide. *Journal of Hazardous Materials* 2009b; 166: 407-414.

553 Xue X, Hanna K, Despas C, Wu F, Deng N. Effect of chelating agent on the oxidation
554 rate of PCP in the magnetite/H₂O₂ system at neutral pH. *Journal of Molecular*
555 *Catalysis A: Chemical* 2009c; 311: 29-35.

556 Yan J, Lei M, Zhu L, Anjum MN, Zou J, Tang H. Degradation of sulfamonomethoxine
557 with Fe₃O₄ magnetic nanoparticles as heterogeneous activator of persulfate.
558 *Journal of Hazardous Materials* 2010; 186: 1398-1404.

559 Zorita S, Mårtensson L, Mathiasson L. Occurrence and removal of pharmaceuticals in a
560 municipal sewage treatment system in the south of Sweden. *Science of The Total*
561 *Environment* 2009; 407: 2760-2770.

Table

Table 1- Degradation products detected by LC and confirmed by MS

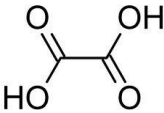
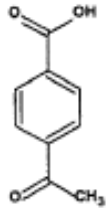
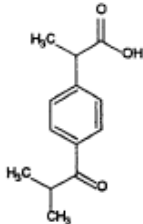
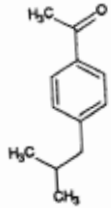
Product	Structure
Oxalic acid	 <p>The chemical structure of oxalic acid is shown as a central carbon-carbon bond. Each carbon is double-bonded to an oxygen atom and single-bonded to a hydroxyl group (-OH).</p>
4-acetylbenzoic acid	 <p>The chemical structure of 4-acetylbenzoic acid consists of a benzene ring with a carboxylic acid group (-COOH) at the top position and an acetyl group (-COCH₃) at the bottom position, in a para relationship.</p>
Oxo-ibuprofen	 <p>The chemical structure of oxo-ibuprofen features a central benzene ring. At the top position, there is a propanoic acid side chain (-CH₂-CH₂-COOH). At the bottom position, there is an isobutyryl side chain (-CH₂-CO-CH(CH₃)₂).</p>
4-IBAP	 <p>The chemical structure of 4-IBAP (4-isobutylacetophenone) consists of a benzene ring with an acetyl group (-COCH₃) at the top position and an isobutyl group (-CH₂-CH₂-CH(CH₃)₂) at the bottom position, in a para relationship.</p>

Figure captions

Figure 1: (a) XRD diffractogram (b) SEM and (c) TEM images of the Fe_3O_4 used.

Figure 2: (a) IBP sorption onto Fe_3O_4 vs pH. $[\text{Fe}_3\text{O}_4] = 1 \text{ g/L}$; $[\text{IBP}] = 0.1 \text{ mM}$; $T = 20 \pm 1 \text{ }^\circ\text{C}$. (b) Sorption isotherms of IBP onto Fe_3O_4 . $[\text{Fe}_3\text{O}_4] = 1 \text{ g/L}$; $T = 20 \pm 1 \text{ }^\circ\text{C}$, $\text{pH } 6.6 \pm 0.1$; $t = 12 \text{ hrs}$. The line represents the Freundlich model.

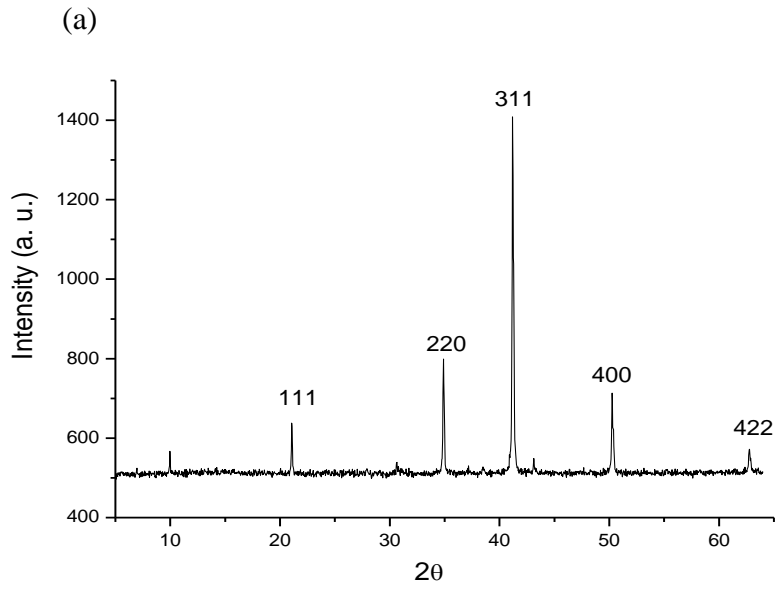
Figure 3: (a) Removal profile of IBP at various H_2O_2 concentrations $[\text{H}_2\text{O}_2]$: (\square) 1 mM, (Δ) 5 mM and (\circ) 10 mM; and in presence of fixed Fe^{2+} concentration $[\text{Fe}^{2+}] = 1 \text{ mM}$, $[\text{H}_2\text{O}_2]$: (\blacksquare) 1 mM, (\blacktriangle) 5 mM and (\bullet) 10 mM. (b) Removal profile of IBP at various PS concentrations in the presence of fixed Fe^{2+} concentration $[\text{Fe}^{2+}] = 1 \text{ mM}$, $[\text{PS}]$: (\circ) 0.5 mM (\square) 1 mM and (Δ) 2.57 mM. $[\text{IBP}] = 0.1 \text{ mM}$; $T = 20 \pm 1 \text{ }^\circ\text{C}$.

Figure 4: (a) Oxidation of IBP by H_2O_2 or (b) $\text{Na}_2\text{S}_2\text{O}_8$ in the presence and absence of iron species; (Δ) absence of iron, (\square) $[\text{Fe}_3\text{O}_4] = 1 \text{ gL}^{-1}$, (\blacktriangle) $[\text{Fe}^{2+}] = 1 \text{ mM}$. $[\text{IBP}] = 0.1 \text{ mM}$; $[\text{oxidant}] = 1 \text{ mM}$; $T = 20 \pm 1 \text{ }^\circ\text{C}$.

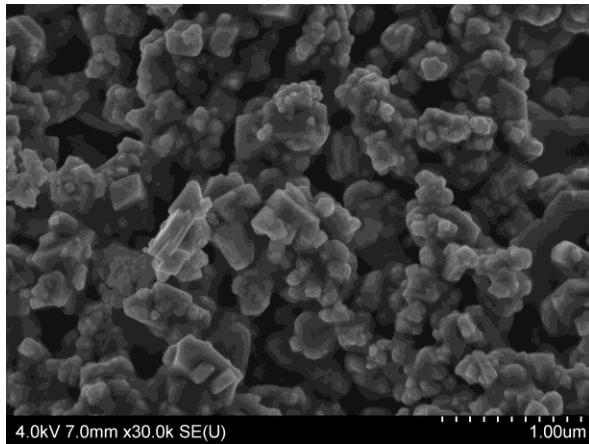
Figure 5: Oxidation of IBP in the presence of (\blacklozenge) $[\text{H}_2\text{O}_2] = 10 \text{ mM}$, (\bullet) $[\text{Na}_2\text{S}_2\text{O}_8] = 10 \text{ mM}$, (\blacktriangle) $[\text{H}_2\text{O}_2] = 10 \text{ mM} + [\text{Fe}_3\text{O}_4] = 1 \text{ gL}^{-1}$ and (\blacksquare) $[\text{Na}_2\text{S}_2\text{O}_8] = 10 \text{ mM} + [\text{Fe}_3\text{O}_4] = 1 \text{ gL}^{-1}$. $[\text{IBP}] = 0.1 \text{ mM}$; $T = 20 \pm 1 \text{ }^\circ\text{C}$.

Figure 6: COD removal of IBP in the absence of iron species and presence of Fe^{2+} .

Figure 7: **Right axis:** Removal of IBP with PS activated by Fe^{2+} (\blacktriangle). **Left axis:** Degradation product formed at retention time 13.2 min during removal of IBP with PS activated by Fe^{2+} (Δ). $[\text{IBP}] = 0.1 \text{ mM}$; $[\text{PS}] = 1 \text{ mM}$; $T = 20 \pm 1 \text{ }^\circ\text{C}$; $t = 1 \text{ hr}$.



(b)



(c)

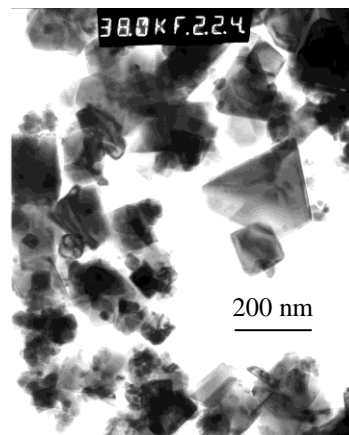


Figure 2

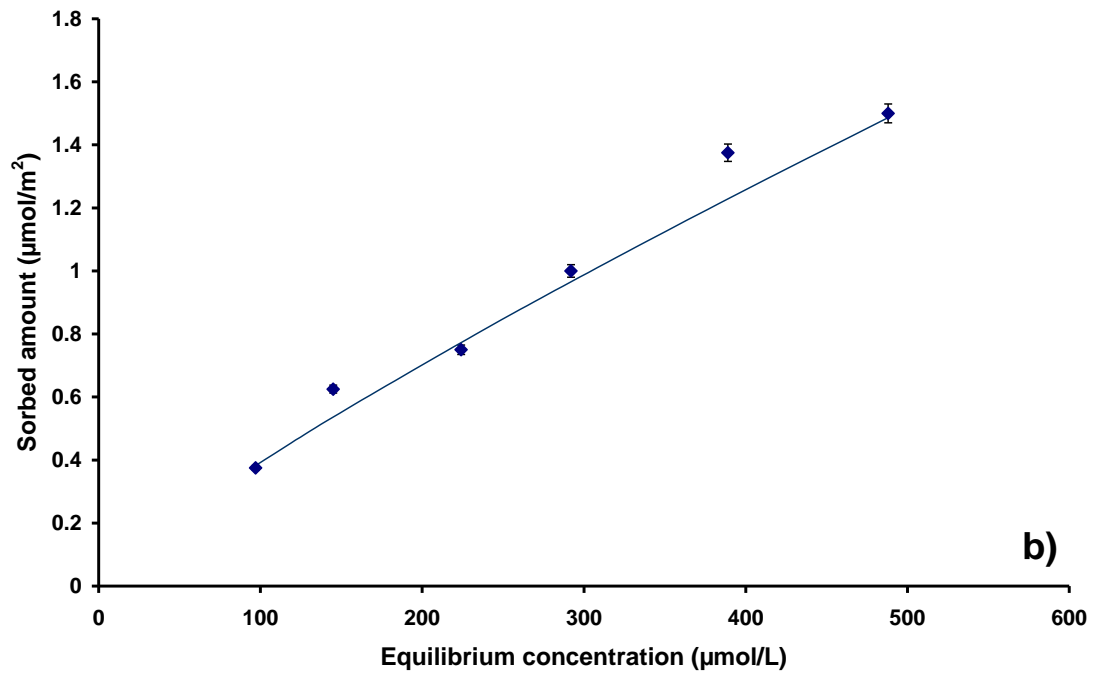
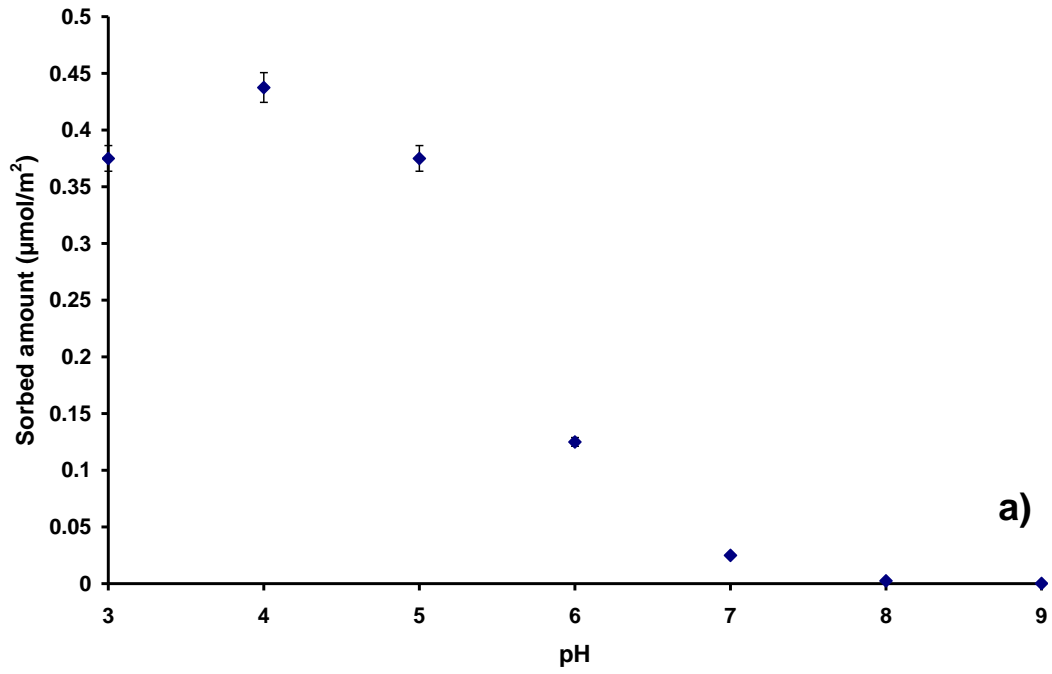


Figure 3

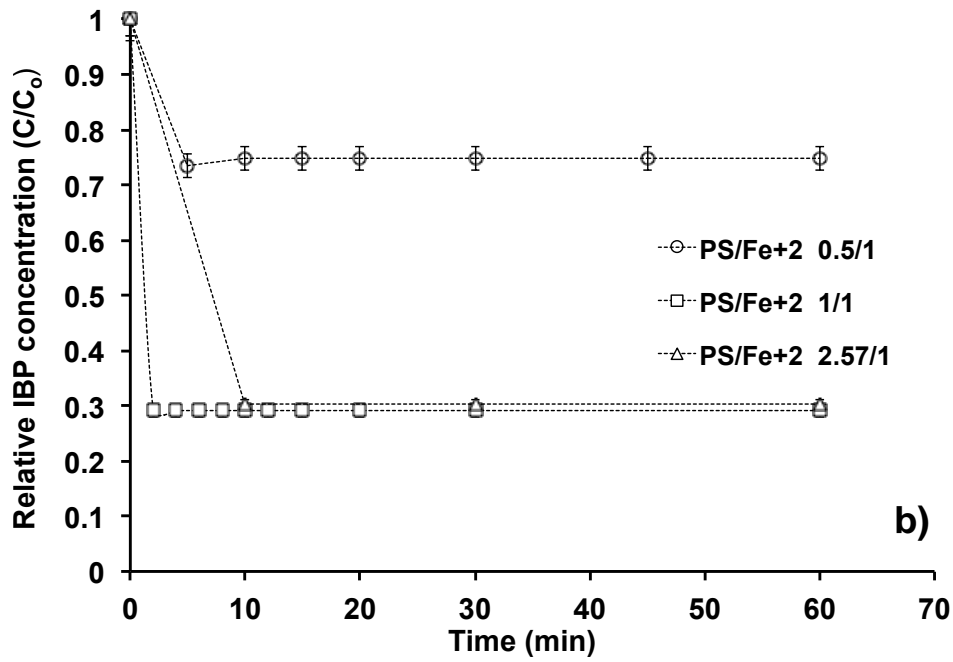
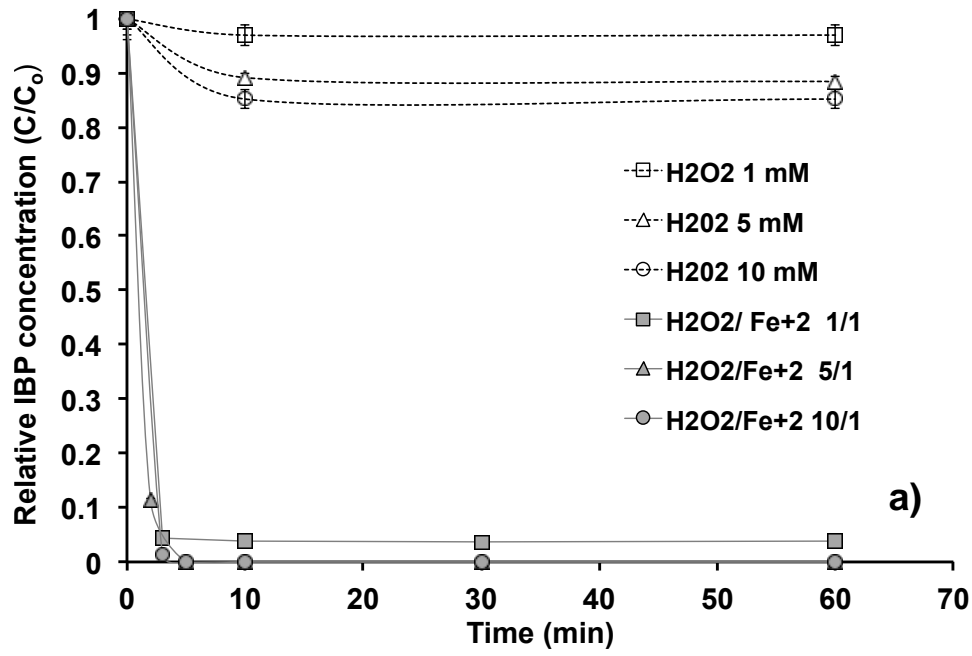


Figure 4

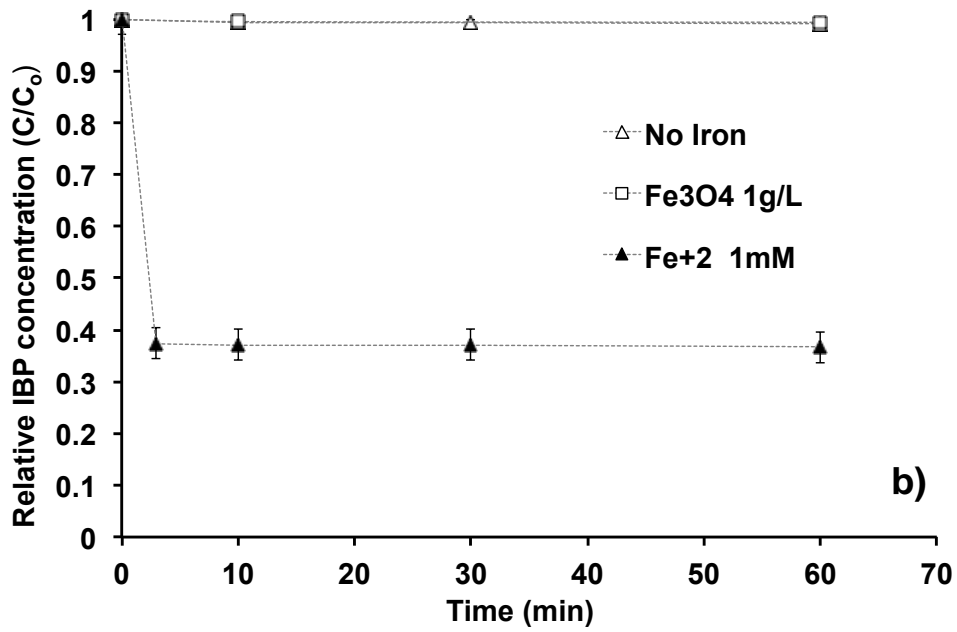
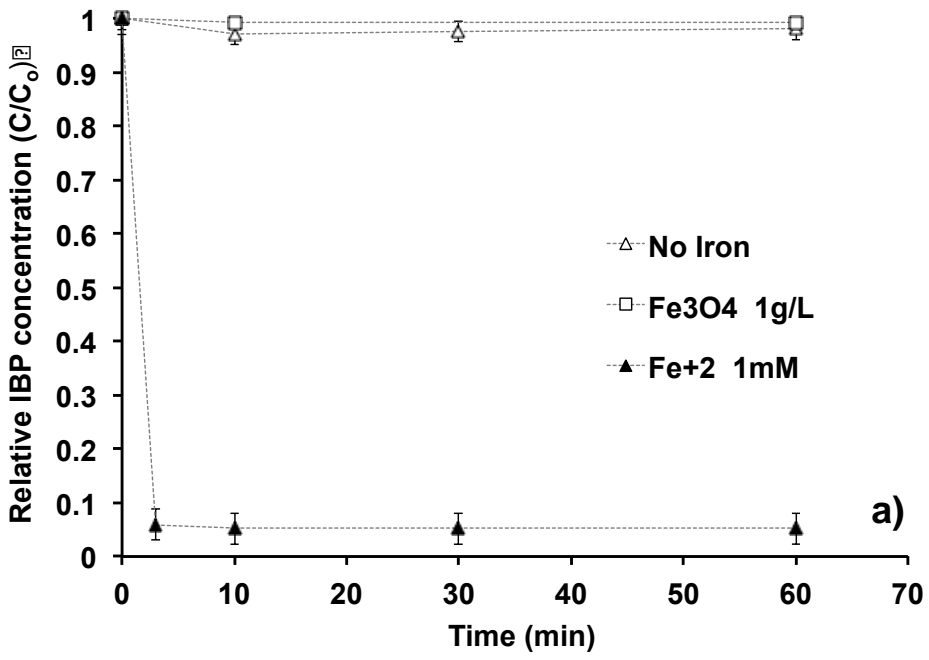


Figure 5

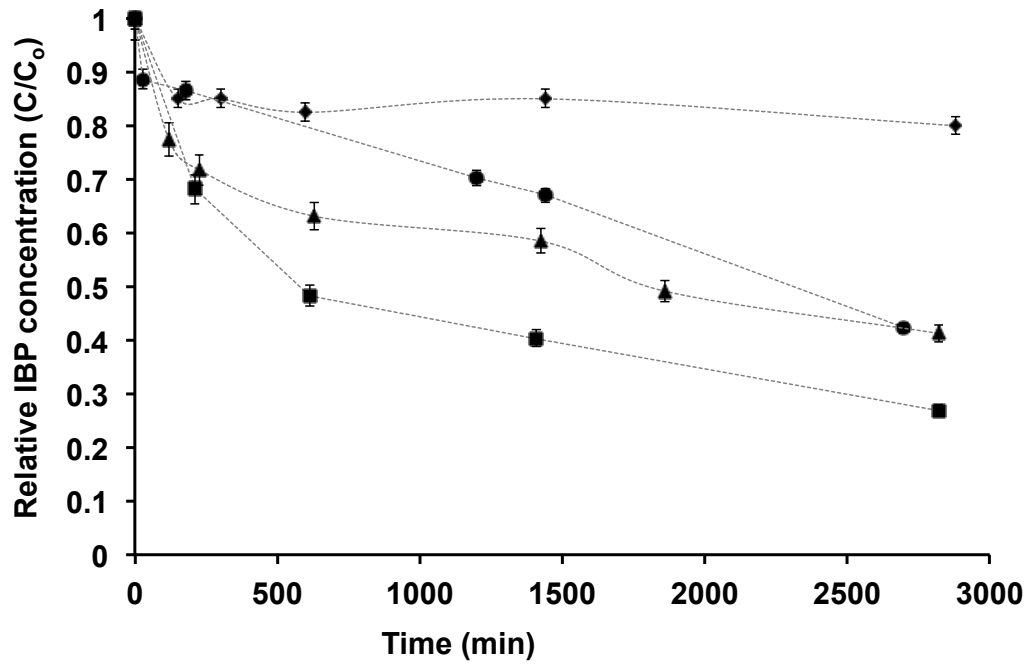


Figure 6

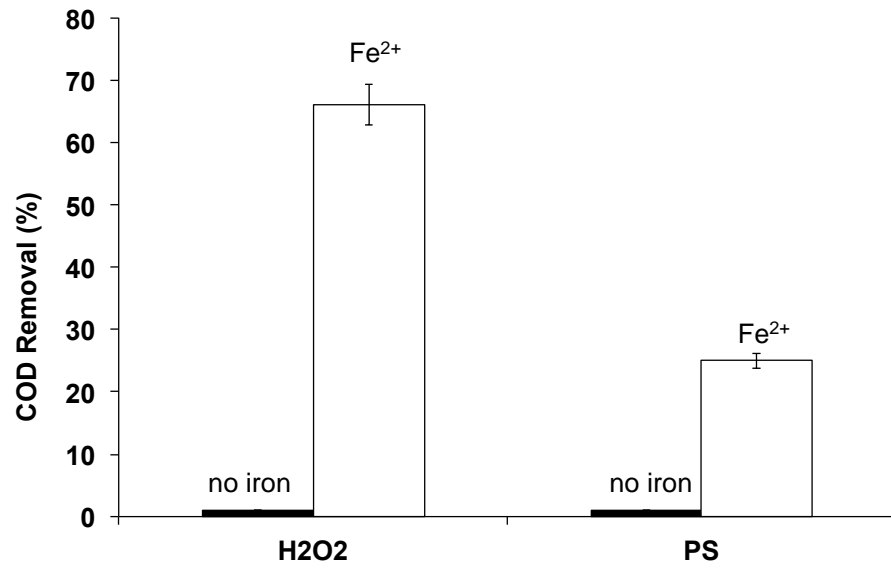


Figure 7

